Sustainable Energy & Fuels

ROYAL SOCIETY OF CHEMISTRY

PAPER

View Article Online
View Journal | View Issue

Check for updates

Cite this: *Sustainable Energy Fuels*, 2023, 7, 3454

Visible-light driven photocatalytic CO_2 reduction promoted by organic photosensitizers and a Mn(I) catalyst†

Elena Bassan, [ab] Rei Inoue,[c] David Fabry,[c] Francesco Calogero,[ab] Simone Potenti, [ad] Andrea Gualandi, [ab] Pier Giorgio Cozzi, [ab] Kei Kamogawa,[c] Paola Ceroni, *[ab] Yusuke Tamaki *[c] and Osamu Ishitani *[ce]

Photocatalytic systems for CO_2 reduction can greatly benefit from the development of fully organic photoredox sensitizers, so as to move away from the use of rare elements. In this study, a series of organic molecules, displaying thermally activated delayed fluorescence (TADF) containing diphenylamine (**4DPAIPN**, **3DPAFIPN**) or carbazole (**5CzBN**, **4CzIPN**, **3CzClIPN**) moieties as electron donating groups were systematically investigated as photoredox sensitizers for CO_2 reduction, coupled with a Mn(I)-complex as the catalyst (**Mn**). All of the TADF dyes were reductively quenched by BIH in triethanolamine (TEOA)–*N*,*N*-dimethylacetoamide solutions. However, their photocatalytic performances were markedly different. **5CzBN**, **4CzIPN**, and **3CzClIPN** did not work as photosensitizers in the studied photocatalytic system because of low absorbance in the visible region and/or low reducing power of their one-electron reduced species. On the other hand, TADF molecules possessing diphenylamine groups are characterized by stronger absorption in the visible region and their one-electron reduced species have stronger reducing power. In particular, **4DPAIPN** proved to be the best performing photosensitizer when using a molar ratio of photosensitizer : catalyst = 1 : 1 and a 470 nm LED source, yielding $TON_{CO+HCOOH}$ > 650 and $\Phi_{CO+HCOOH} = 22.8 \pm 1.5\%$.

Received 27th April 2023
Accepted 12th June 2023

DOI: 10.1039/d3se00546a

rsc.li/sustainable-energy

Open Access Article. Published on 27 June 2023. Downloaded on 2/10/2026 4:20:43 PM.
This article is licensed under a Creative Commons Attribution-NonCommercial 3.0 Unported Licence.

Introduction

The depletable nature of fossil fuels and the release of enormous amounts of CO_2 into the atmosphere (about 34 Gt per year) upon their combustion have prompted mankind to devise artificial photosynthetic systems that are able to store sunlight into high-energy products known as solar fuels.[1] The ultimate goal is therefore to produce fuels by using low-energy and widely available feedstock, such as water and carbon dioxide, and sunlight as the sole energy source.[2,3] To reach this goal an artificial photosynthetic system should comprise a photosensitizer (PS) that efficiently absorbs visible light for initiating electron transfer, a catalyst (CAT) that is able to store electrons or holes and drive multielectronic redox processes, and a sacrificial electron donor (S) that is irreversibly oxidized (Fig. 1).[4,5] This approach simplifies the process and facilitates the study of the kinetics of the relevant processes and of the photo- and chemical stability of the different components. In such systems, the photosensitizer should be characterized by strong visible-light absorption, photostability, a long lifetime of the involved excited state and appropriate redox potentials. On the other hand, a catalyst should be able to accumulate

[a]*Dipartimento di Chimica "Giacomo Ciamician", Alma Mater Studiorum – Università di Bologna, Via Selmi 2, 40126 Bologna, Italy. E-mail: paola.ceroni@unibo.it*

[b]*Center for Chemical Catalysis – C3, Alma Mater Studiorum – Università di Bologna, Via Selmi 2, 40126 Bologna, Italy*

[c]*Department of Chemistry, School of Science, Tokyo Institute of Technology, 2-12-1-NE-1 O-okayama, Meguro-ku, Tokyo 152-8550, Japan. E-mail: tamaki@chem.titech.ac.jp; ishitani@chem.titech.ac.jp*

[d]*Laboratorio SMART, Scuola Normale Superiore, Piazza dei Cavalieri 7, 56126, Pisa, Italy*

[e]*Department of Chemistry, Graduate School of Advanced Science and Engineering, Hiroshima University, 1-3-1 Kagamiyama, Higashi-Hiroshima, Hiroshima 739-8526, Japan*

† Electronic supplementary information (ESI) available: Synthetic procedures, additional mechanistic studies. See DOI: https://doi.org/10.1039/d3se00546a

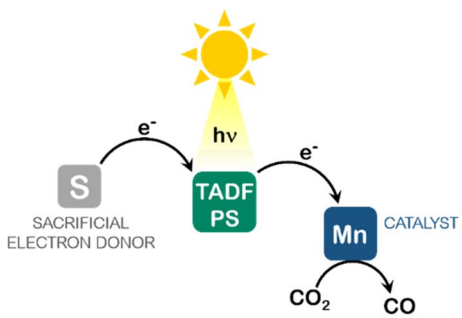

Fig. 1 Schematic representation of the studied system.

This journal is © The Royal Society of Chemistry 2023

Open Access Article. Published on 27 June 2023. Downloaded on 2/10/2026 4:20:43 PM.
This article is licensed under a Creative Commons Attribution-NonCommercial 3.0 Unported Licence.

electrons, have a high selectivity towards CO_2 reduction, and be chemically stable under the reaction conditions.

Given these requirements, most systems capable of reducing CO_2 traditionally rely on heavy-metal complexes (*e.g.* Ru and Ir) as photosensitizers,[6,7] whereas a large-scale application should desirably be based on abundant and non-toxic compounds. For this reason, research has recently been focusing on the development of both photosensitizers[8] and catalysts[9–12] that are either based on abundant metals or consist of purely organic compounds. Recently, a copper(II) purpurin complex,[13] and mononuclear and dinuclear copper(I) complexes[14–20] have for instance been utilized as photosensitizers in order to achieve the photochemical reduction of CO_2. Although Zn porphyrins have been used as photosensitizers for CO_2 reduction, their efficiency and durability are relatively low, especially in systems coupled with abundant-metal complexes as catalysts.[21,22] Attempts at using metal-free photosensitizers to drive the photoreduction of CO_2 initially included the use of cyanoanthracene[23] and *p*-terphenyl[24–26] dyes, which have the disadvantage of a short excited-state lifetime and absorption maxima located in the UV region. More recently, organic photosensitizers with stronger visible light absorption such as purpurin derivatives[27–29] or the ability to populate their long-lived triplet excited state like phenazine[30,31] have been employed.

A long excited-state lifetime is an essential feature of a photosensitizer since it increases the efficiency of bimolecular interactions, such as reductive quenching by a sacrificial electron donor. This feature is commonly found in transition metal complexes, as in the case of $[Ru(bpy)_3]^{2+}$.[32] Nonetheless, strategies have been devised to induce intersystem crossing (ISC) in organic chromophores[33–35] like the synthesis of compounds that are characterized by highly twisted electron donating and electron accepting units.[36–38] In this way, it is possible to minimize the energy gap (ΔE) between the lowest singlet excited state (S_1) and the lowest triplet excited state (T_1) promoting intersystem crossing (from S_1 to T_1) and reverse intersystem crossing (RISC) (from T_1 to S_1), and thus gives rise to thermally activated delayed fluorescence (TADF) (Fig. 2). On top of enabling the population of a long-lived excited state, TADF compounds allow the tuning of redox potentials thanks to the strong localization of their HOMO and LUMO orbitals.[38] Despite an extensive use of this class of organic dyes in photoredox catalysis,[39,40] only one organic TADF molecule, *i.e.*, **4CzIPN** (Chart 1), has been used as a photosensitizer for the reduction

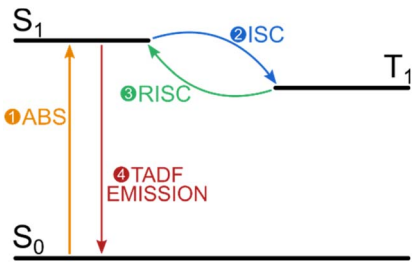

Fig. 2 Jablonski diagram illustrating the relevant steps for TADF emission.

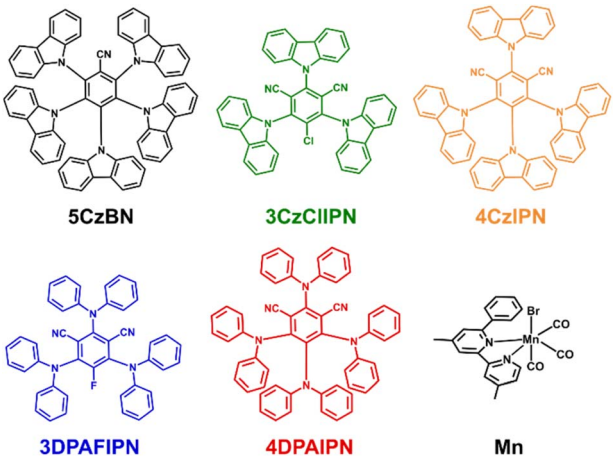

Chart 1 Structures and abbreviations of the organic TADF dyes and of the Mn(I) complex.

of CO_2.[41–45] In order to construct highly efficient and durable photocatalytic systems using organic TADF dyes, improvements are needed in terms of stronger and red-shifted absorption of visible light, stronger oxidation power in the excited state, and higher stability of the reduced state. For example, in the case of **4CzIPN**, its molar absorption coefficient is negligible at wavelengths longer than 470 nm, and this implies that an excess of **4CzIPN** compared to the amount of catalyst is used (typical molar ratios: 5–10 : 1).[41–45] Moreover, addition of an excess of PS frequently induces its decomposition, owing to the accumulation of its reduced form in the reaction solution. Therefore, although the turnover number (TON) based on the used CAT is high (in the order of 10^3), TON based on the used PS is much lower (*ca.* 10^2) and the reported quantum yields of CO_2 reduction are less than 5%.[46]

In this work, we investigate the ability of five organic TADF molecules to work as PSs in a three-component artificial photosynthetic system for photocatalytic CO_2 reduction. These were coupled with a new earth-abundant Mn(I) catalyst[46,47] (Chart 1), which has a sterically hindered phenyl group close to the central Mn for suppressing reductive dimerization,[47,48] and with 1,3-dimethyl-2-phenyl-2,3-dihydro-1*H*-benzimidazole (BIH)[49] as the sacrificial electron donor to successfully develop an efficient and durable photocatalytic system without using heavy metals. Comparison of the photophysical and electrochemical properties of the chromophores allowed the rationalization of the different catalytic activities, which reach $TON_{CO+HCOOH} > 650$ and $\Phi_{CO+HCOOH} = 22.8 \pm 1.5\%$ in the case of **4DPAIPN**.

Results and discussion

Chart 1 shows the investigated TADF photosensitizers together with the Mn(I) complex used as the catalyst, which has a phenyl group at the 6 position of the 4,4′-dimethyl-2,2′-bipyridine ligand in order to suppress dimerization of its reduced state.[48]

Fig. 3 shows the absorption spectra of the TADF chromophores measured in *N*,*N*-dimethylacetamide (DMA). All

Open Access Article. Published on 27 June 2023. Downloaded on 2/10/2026 4:20:43 PM.
This article is licensed under a Creative Commons Attribution-NonCommercial 3.0 Unported Licence.

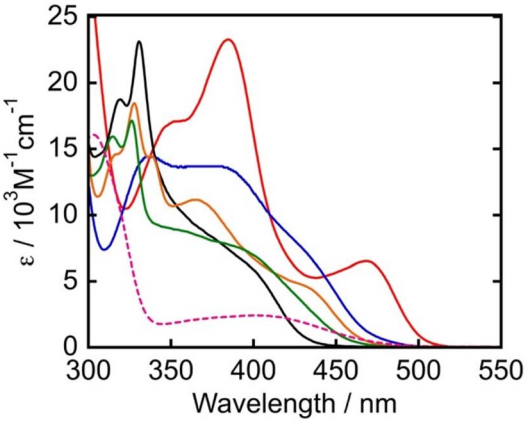

Fig. 3 UV-vis absorption spectra of PSs in DMA (**4DPAIPN**: red, **3DPAFIPN**: blue, **5CzBN**: black, **4CzIPN**: orange, **3CzClIPN**: green). The pink dashed line indicates the UV-vis absorption spectrum of **Mn** in DMA.

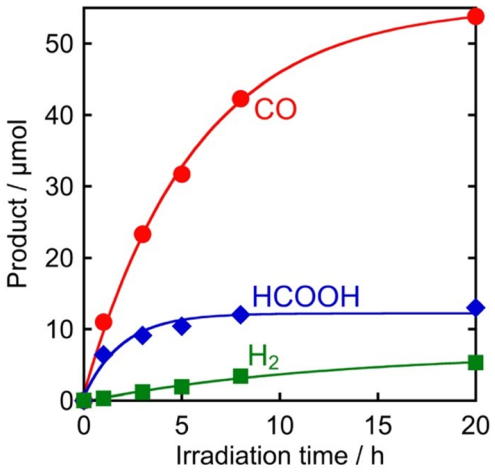

Fig. 4 Photocatalytic production of CO (•), HCOOH (◆), and H_2 (■) using **3DPAFIPN** as a photosensitizer: CO_2-saturated DMA solutions (2 mL) containing **3DPAFIPN** (250 μM), **Mn** (50 μM), BIH (0.1 M), and TEOA (1.5 M) were irradiated at $\lambda_{ex} = 440$ nm.

compounds present broad absorption bands in the visible region attributable to charge-transfer transitions from the electron donating diphenylamine (DPA) or carbazole (Cz) moieties to the electron accepting cyanobenzene unit. The absorption onsets were observed in the order of **4DPAIPN** > **3DPAFIPN** > **4CzIPN** > **3CzClIPN** > **5CzBN**. The red-shifted absorption of **4DPAIPN** and **3DPAFIPN** compared to their carbazole analogues is attributed to the more electron-rich nature of DPA moieties compared to Cz moieties. This leads to a destabilization of the HOMO, resulting in smaller transition energies for visible-light absorption. In particular, **4DPAIPN** is characterized by an absorption onset at 516 nm (ε = 100 M^{-1} cm^{-1}). The photophysical properties of the PSs are summarized in Table 1.

All these organic PSs exhibit emission spectra in the visible region. From time-resolved emission measurements, all of these emission decays can be fitted with double exponential functions. The short components (in the range of ns) are attributed to prompt fluorescence, while the longer components (in the range of μs) are due to TADF (Table 1). For example, the TADF emission of **4DPAIPN** displays a lifetime of 84 μs, which is long enough to function as a photosensitizer in bimolecular quenching processes. Interestingly, for all of the studied TADF dyes, strong emission quenching is observed in the presence of BIH (0.1 M)[49] and triethanolamine (TEOA, 1.5 M) (quenching efficiencies η_q = 93–98%, Fig. S1†), which are the same conditions used in the photocatalytic reactions described below. These results indicate that the excited states of all of these organic compounds are quenched by BIH and/or TEOA. Therefore, these organic compounds can possibly work as photosensitizers to drive photocatalytic CO_2 reduction.

Fig. 3 also shows the absorption spectrum of **Mn** in DMA. Since the onset of its absorption band is 501 nm, irradiation with visible light at $\lambda_{ex} \leq 501$ nm can potentially induce photodecomposition of **Mn**. Consequently, different reaction conditions (in terms of light sources and concentrations) were employed for testing the organic chromophores' ability of promoting photocatalytic CO_2 reduction. In the first case, blue light LED peaked at 440 nm was used to irradiate a CO_2-saturated DMA solution containing **PS** (250 μM), **Mn** (50 μM), BIH (0.1 M) and TEOA (1.5 M). Since **Mn** also absorbs light at 440 nm ($\varepsilon = 1.50 \times 10^3$ M^{-1} cm^{-1}), 5-times higher concentrations of PSs

Table 1 Photophysical properties of PSs and **Mn** in DMA[a]

	$\varepsilon/10^3$ M^{-1} cm^{-1}		λ_{abs}/nm					
	(440 nm)	(470 nm)	(ε = 100)	λ_{em}/nm	τ_{PF}[b]/ns	τ_{TADF}[c]/μs	Φ_{em}[d]/%	η_q[e]/%
4DPAIPN	5.29	6.50	516	527	2.9	84	48.9	93
3DPAFIPN	5.93	1.11	498	536	3.6	43	16.0	93
5CzBN	0.31	0.05	454	515	24	10	33.9	98
4CzIPN	3.88	0.42	486	552	21	2.1	30.0	98
3CzClIPN	2.15	0.19	478	554	13	32	9.9	94
Mn	1.50	0.48	501	—	—	—	—	—

[a] The estimated errors in the photophysical measurements are reported in the ESI. [b] Lifetime of prompt fluorescence. [c] Lifetime of TADF emission. [d] Emission quantum yield in an Ar atmosphere. [e] Quenching fraction of the emission calculated from $\eta_q = 1 - I/I^0$; I: emission intensity in Ar-saturated DMA containing both TEOA (1.5 M) and BIH (0.1 M); I^0: emission intensity in Ar-saturated DMA.

 This journal is © The Royal Society of Chemistry 2023

Open Access Article. Published on 27 June 2023. Downloaded on 2/10/2026 4:20:43 PM.
This article is licensed under a Creative Commons Attribution-NonCommercial 3.0 Unported Licence.

Table 2 Photocatalytic reactions using PSs and the Mn(I) catalyst with a 5 : 1 ratio[a]

		Product/μmol			TON^{PS}			TON^{Mn}		
Entry		CO	HCOOH	H_2	CO	HCOOH	H_2	CO	HCOOH	H_2
1	**4DPAIPN**	40.8	9.7	5.5	82	19	11	408	97	55
2	**3DPAFIPN**	53.8	13.0	5.3	108	26	11	538	130	53
3	**5CzBN**	3.1	1.1	0.3	6	2	<1	31	11	3
4	**4CzIPN**	0.4	<0.1	1.2	<1	<1	2	4	<1	11
5	**3CzClIPN**	0.4	<0.1	0.3	<1	<1	<1	4	<1	3

[a] CO_2-saturated DMA solutions (2 mL) containing PS (250 μM), **Mn** (50 μM), BIH (0.1 M), and TEOA (1.5 M) were irradiated using LED light at λ_{ex} = 440 nm for 20 h.

were used to limit the percentage of light absorbed by **Mn** and thus reduce its decomposition. For example, in the case of **3DPAFIPN** (Fig. 4), after 20 h of irradiation, 53.8 μmol of CO and 13.0 μmol of HCOOH were produced along with 5.3 μmol of H_2, which corresponds to turnover numbers based on **3DPAFIPN** of $TON_{CO}^{3DPAFIPN} = 108$ and $TON_{HCOOH}^{3DPAFIPN} = 26$ and TON based on **Mn** of $TON_{CO}^{Mn} = 538$ and $TON_{HCOOH}^{Mn} = 130$. HCOOH formation stopped rapidly after approximately 3–5 h of irradiation, although CO kept on being produced even at longer irradiation times. The results of the photocatalytic reactions carried out under the same conditions as shown in Fig. 4 but using the other organic photosensitizers are summarized in Table 2. High photocatalytic activity was also observed when using **4DPAIPN** as PS, but its performance was slightly lower under these reaction conditions compared to that observed when using **3DPAFIPN**. On the other hand, utilization of the PSs possessing Cz moieties gave poor results in the photocatalytic reduction of CO_2. Noteworthily, **4CzIPN**, which was used as the PS for photocatalytic CO_2 reduction in previous studies,[41–45] did not show photocatalytic ability for CO_2 reduction in our system. The lack of activity observed for **4CzIPN** and **3CzClIPN** can be explained by comparison between the first reduction potential of **Mn** (E_p(**Mn**/**Mn**$^{\bullet-}$) = −1.83 V *vs.* Fc^+/Fc) and the reduction potentials of **4CzIPN** ($E_{1/2}$(PS/PS$^{\bullet-}$) = −1.72 V *vs.* Fc^+/Fc) and **3CzClIPN** (−1.61 V *vs.* Fc^+/Fc) (Fig. 5 and Table 3). Indeed, these two reduction potentials are more positive than the first reduction wave of **Mn**, therefore the electron transfer processes from one-electron reduced **4CzIPN** and **3CzClIPN** to **Mn** are endothermic

Table 3 Electrochemical properties of PSs and CAT

PS	$E_{1/2}$/V *vs.* Fc^+/Fc
4DPAIPN	−2.08
3DPAFIPN	−1.94
5CzBN	−1.99
4CzIPN	−1.72
3CzClIPN	−1.61
CAT	E_p/V *vs.* Fc^+/Fc
Mn	−1.83

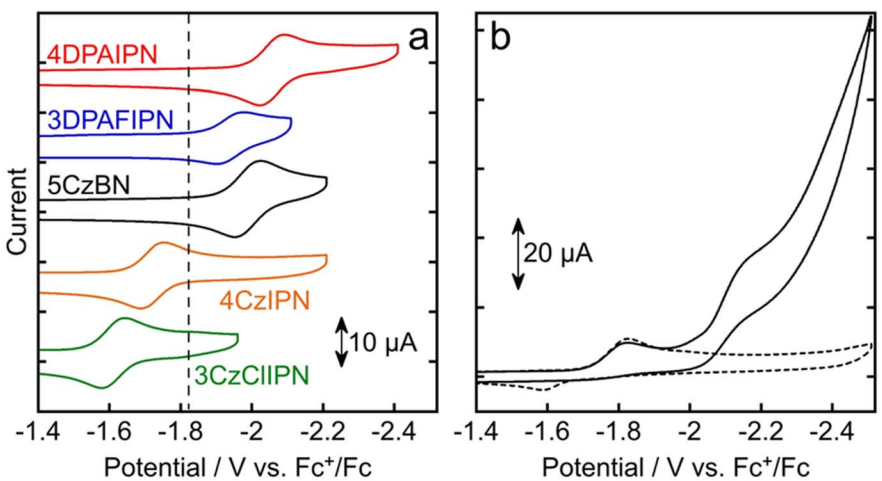

Fig. 5 Cyclic voltammograms of (a) **4DPAIPN** (red line), **3DPAFIPN** (blue line), **5CzBN** (black line), **4CzIPN** (orange line), and **3CzClIPN** (green line) measured in Ar-saturated DMA containing Et_4NBF_4 (0.1 M) as the supporting electrolyte with a Ag/$AgNO_3$ (10 mM) reference electrode, and (b) of **Mn** in Ar-saturated (broken line) and CO_2-saturated (solid line) solutions using the same electrolyte and reference electrode. The Fc^+/Fc redox couple was also measured and taken as the standard. Scan rate was 0.2 V s^{-1}. The dashed vertical line in (a) indicates the first reduction potential of **Mn**: E_p(**Mn**/**Mn**$^{\bullet-}$) = −1.83 V.

Open Access Article. Published on 27 June 2023. Downloaded on 2/10/2026 4:20:43 PM.
This article is licensed under a Creative Commons Attribution-NonCommercial 3.0 Unported Licence.

Table 4 Photocatalytic CO_2 reduction using an organic photosensitizer and **Mn** at 1 : 1 ratio[a]

			Product/μmol			TON[b]		
Entry	Photosensitizer	λ_{ex}/nm	CO	HCOOH	H_2	CO	HCOOH	H_2
1	**4DPAIPN**	440	35.7	10.2	7.1	357	102	71
2	**3DPAFIPN**		13.3	5.5	1.0	133	55	10
3	**4DPAIPN**	470	47.6	18.9	2.9	476	189	29
4	**3DPAFIPN**		4.3	2.5	0.5	43	25	5

[a] CO_2-saturated DMA solutions (2 mL) containing PS (50 μM), **Mn** (50 μM), BIH (0.1 M), and TEOA (1.5 M) were irradiated using LED light at λ_{ex} = 440 nm or 470 nm for 20 h. [b] In the case of entry 1, the same experiments were repeated three times and the results including the experimental errors are as follows: $TON_{CO} = 476 \pm 20$, $TON_{HCOOH} = 189 \pm 15$, $TON_{H_2} = 29 \pm 10$.

and cannot take place. In contrast, **4DPAIPN**, **3DPAFIPN**, and **5CzBN** possess more negative reduction potentials compared to **Mn**, and this makes the reduction of the catalyst thermodynamically allowed.

5CzBN exhibited much lower photocatalytic activity compared to **3DPAFIPN** and **4DPAIPN** because of its lower molar absorption coefficient at 440 nm (Table 1). In fact, under the tested experimental reaction conditions the absorbance of **5CzBN** at 440 nm is even less compared to that of **Mn** (Fig. S2†). Consequently, photosensitive **Mn** is exposed to light and this leads to its decomposition and interruption of catalysis.

Given that **4DPAIPN** and **3DPAFIPN** have much stronger absorbances at 440 nm and suitable redox potentials, we focused only on these two PSs in order to further optimize the reaction conditions. First, the concentrations of PSs were decreased to 50 μM, so that the ratio of PS : **Mn** was 1 : 1 (entries 1 and 2 in Table 4). Under these conditions, the system using **4DPAIPN** maintained good photocatalytic activity ($TON_{CO} = 357$ and $TON_{HCOOH} = 102$), while photocatalysis in the presence of **3DPAFIPN** drastically decreased ($TON_{CO} = 133$ and $TON_{HCOOH} = 55$), suggesting that the stability of **3DPAFIPN** is less compared to **4DPAIPN** during the reaction. Second, a longer wavelength (λ_{ex} = 470 nm) was employed for irradiating solutions containing PS : **Mn** = 1 : 1 (50 μM each, entries 3 and 4 in Table 4). In this case, the superior performance of **4DPAIPN** compared to **3DPAFIPN** is even more pronounced, as expected from the higher absorbance of **4DPAIPN** ($\varepsilon_{470\ nm} = 6.50 \times 10^3\ M^{-1}\ cm^{-1}$) compared to that of **3DPAFIPN** ($\varepsilon_{470\ nm} = 1.11 \times 10^3\ M^{-1}\ cm^{-1}$) at wavelengths longer that 450 nm. Fig. 6 shows the formation of CO_2-reduction products over time using 50 μM of **4DPAIPN** and **Mn**. In the initial stage, a larger amount of HCOOH was produced in comparison to that of CO, followed by a halt in HCOOH formation after 5 h of irradiation. In contrast, formation of CO continued even after 20 h of irradiation and CO becomes the major product. After 20 h of irradiation, 47.6 μmol of CO and 18.9 μmol of HCOOH were formed along with 2.9 μmol of H_2, which corresponds to $TON_{CO} = 476$, $TON_{HCOOH} = 189$, and $TON_{H_2} = 29$. These results are slightly larger than those obtained under irradiation at 440 nm because **Mn** has very little absorption at 470 nm, resulting in reduced photodegradation of the catalyst. The fact that formation of HCOOH stopped after 5 h of irradiation while CO continued forming even after 20 h suggests that different manganese complexes derived from **Mn** (and possibly **Mn** itself) form during the reaction. Since blue colour was not detected in the reaction solution during the photocatalytic reaction, the reductive dimer of the Mn complex did not probably contribute to the photocatalytic CO_2 reduction.[12,47,48] The reaction mechanism related to **Mn** and its derivatives in the photocatalytic reactions is currently under investigation in our laboratory.

In order to further characterize the system involving **4DPAIPN** and Mn (1 : 1), the quantum yields (Φ) for CO_2 reduction in the initial stage were determined using 480 nm monochromatic light with a light intensity of 5.0×10^{-9} Einstein per s. These were found to be $\Phi_{CO} = 5.9 \pm 0.2\%$ and $\Phi_{HCOOH} = 16.9 \pm 1.3\%$ from the linear production up to 9 h and 4 h of irradiation, respectively (Fig. 7 and S7†). This is the

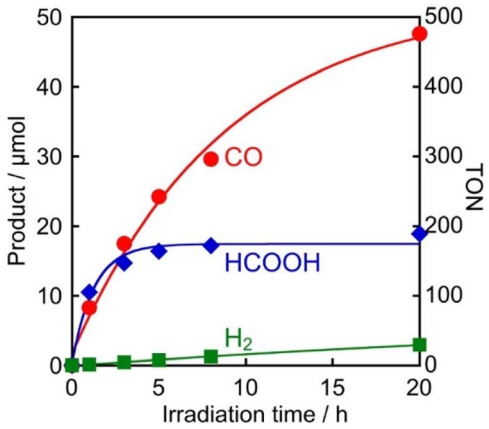

Fig. 6 Photocatalytic production of CO (•), HCOOH (◆), and H_2 (■) using **4DPAIPN** as a photosensitizer: CO_2-saturated DMA solutions (2 mL) containing **4DPAIPN** (50 μM), **Mn** (50 μM), BIH (0.1 M), and TEOA (1.5 M) were irradiated at λ_{ex} = 470 nm.

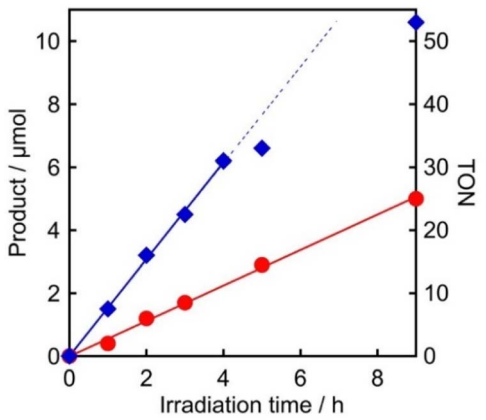

Fig. 7 Photocatalytic production of CO (•) and HCOOH (◆) using **4DPAIPN**: CO_2-saturated DMA solutions (4 mL) containing **4DPAIPN** (50 μM), **Mn** (50 μM), BIH (0.1 M), and TEOA (1.5 M) were irradiated at λ_{ex} = 480 nm. Light intensity = 5.0×10^{-9} Einstein per s.

 This journal is © The Royal Society of Chemistry 2023

Open Access Article. Published on 27 June 2023. Downloaded on 2/10/2026 4:20:43 PM.
This article is licensed under a Creative Commons Attribution-NonCommercial 3.0 Unported Licence.

Table 5 Control experiments for photocatalytic CO_2 reduction[a]

Entry	Absence	Product/μmol (TON) CO	HCOOH	H_2
1	—	47.6 (476)	18.9 (189)	2.9
2[b]	**4DPAIPN**	<0.1 (<1)	n.d.	0.1
3[b]	**Mn**	n.d.	n.d.	<0.1
4[b]	BIH	0.7 (7)	0.4 (4)	<0.1
5[b]	TEOA	6.8 (68)	2.4 (24)	1.5
6[c]	Light irradiation	n.d.	n.d.	n.d.
7[d]	CO_2	n.d.	n.d.	0.7

[a] A CO_2-saturated DMA solution (2 mL) containing **4DPAIPN** (50 μM), **Mn** (50 μM), BIH (0.1 M), and TEOA (1.5 M) was irradiated using 470 nm light for 20 h. [b] Photocatalytic reactions were performed without **4DPAIPN**, **Mn**, BIH, or TEOA, respectively. [c] The solution was placed in the dark for 20 h. [d] An Ar-saturated solution was used.

highest quantum yield of CO_2 reduction using organic photosensitizers, to the best of our knowledge.

Table 5 summarizes the control experiments for the photocatalytic reduction of CO_2 using **4DPAIPN**. In the absence of **4DPAIPN** or **Mn**, no products were formed. Control experiments in the dark or using an Ar-saturated solution yielded no products of photocatalytic CO_2 reduction, as well. Irradiation without BIH led to the formation of much smaller amounts of CO and HCOOH ($TON_{CO} = 7$ and $TON_{HCOOH} = 4$) compared to those with BIH ($TON_{CO} = 476$ and $TON_{HCOOH} = 189$) indicating that BIH mainly functioned as a sacrificial electron donor. In the absence of TEOA, the produced amounts of CO and HCOOH ($TON_{CO} = 68$ and $TON_{HCOOH} = 24$) also decreased. Therefore, the possible roles of TEOA should be as follows: (1) as a base, so as to deprotonate the one-electron oxidized BIH ($BIH^{\bullet+}$) and prevent backward electron transfer from $PS^{\bullet-}$ to $BIH^{\bullet+}$, (2) as a supporting ligand to capture CO_2 into the manganese(I) complex to form carbonate ester species, *i.e.*, Mn–CO_2–OC_2H_4-$N(C_2H_4OH)_2$, which is a catalytic precursor for CO_2 reduction,[50] and (3) as a proton source. These results indicate that **4DPAIPN**, **Mn**, and BIH worked as PS, CAT, and the sacrificial electron donor, respectively for photocatalytic reduction of CO_2.

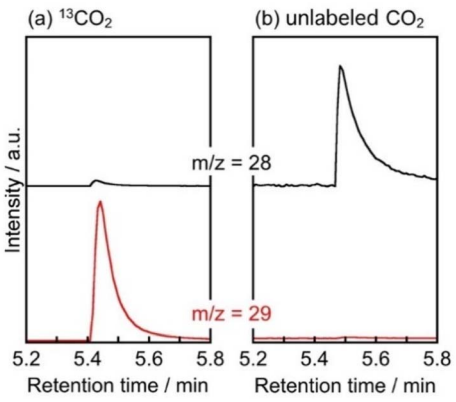

Fig. 8 GC-MS chromatograms of the gas phase after irradiation: a DMA (2 mL) solution containing **4DPAIPN** (250 μM), **Mn** (250 μM), BIH (0.1 M), and TEOA (1.5 M) was irradiated at $\lambda_{ex} = 470$ nm for 20 h under (a) $^{13}CO_2$ or (b) unlabeled CO_2 atmosphere.

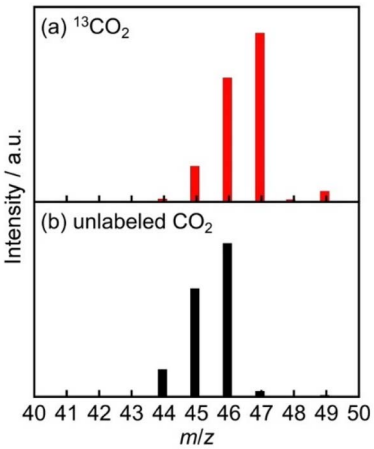

Fig. 9 GC-mass spectra of the liquid phase of the photocatalytic reaction at 8.0 min of retention time: a DMA (2 mL) solution containing **4DPAIPN** (250 μM), **Mn** (250 μM), BIH (0.1 M), and TEOA (1.5 M) was irradiated at $\lambda_{ex} = 470$ nm for 20 h under (a) $^{13}CO_2$ or (b) unlabeled CO_2 atmosphere. The produced HCOOH was extracted from the reaction solution with ethyl acetate and sulfuric acid aqueous solution (experimental details are shown in the ESI†).

In order to confirm that CO and HCOOH were produced *via* reduction of CO_2, isotope labeling experiments using $^{13}CO_2$ (99% ^{13}C content) were performed. Fig. 8 displays the GC-MS chart of the gas phase after the photocatalytic reactions. When working in a $^{13}CO_2$ atmosphere, a strong signal at $m/z = 29$ was observed at 5.5 min of retention time, which is attributed to ^{13}CO, along with a weak signal at $m/z = 28$ attributable to ^{12}CO (Fig. 8a). The ratio between these two signals is 97 : 3. When photocatalyzed under unlabeled CO_2, on the other hand, almost only a signal at $m/z = 28$ was observed (Fig. 8b). For the identification of $H^{13}COOH$ and $H^{12}COOH$, ^1H and ^{13}C NMR have been frequently used. In this photocatalytic system, however, NMR spectroscopy was not applicable probably due to the presence of paramagnetic manganese species. Therefore, HCOOH was extracted from the reaction solution with ethyl acetate and sulfuric acid aqueous solution, and was analyzed using GC-MS (Fig. 9).[51] In the case of an unlabeled CO_2 atmosphere, signals at $m/z = 44$, 45, 46 were observed at 8.0 min of retention time with the relative intensities of 0.18 : 0.71 : 1. Because the retention time and relative intensities of the signals were fairly similar to the reference sample of HCOOH solution, the observed signals are attributed to $H^{12}COOH$ (Fig. 9b). When

Table 6 Quenching rate constants (k_q) and quenching fractions in the presence of each quencher solely (η_q)

Emission	k_q/M^{-1} s^{-1} BIH	TEOA	η_q in the presence of the quencher/% BIH (0.1 M)	TEOA (1.5 M)
PF	2.7×10^9	$<10^7$	44	~0
TADF	1.5×10^8	3.2×10^4	>99	80

Open Access Article. Published on 27 June 2023. Downloaded on 2/10/2026 4:20:43 PM.
This article is licensed under a Creative Commons Attribution-NonCommercial 3.0 Unported Licence.

photocatalyzed in a $^{13}CO_2$ atmosphere, +1-shifted signals attributable to $H^{13}COOH$ were observed at m/z = 45, 46, 47 (Fig. 9a). The relative intensities of these signals were 0.21 : 0.74 : 1. These results clearly indicate that both CO and HCOOH were mostly produced from CO_2.

In order to study the mechanism of the reaction, Stern–Volmer analyses of **4DPAIPN** using BIH and TEOA were performed. Since **4DPAIPN** displays prompt fluorescence (PF) and TADF at the same wavelength (λ_{em} = 527 nm) with significantly different lifetimes (τ_{PF} = 2.9 ns and τ_{TADF} = 84 μs), Stern–Volmer plots using emission lifetimes were performed (Table 6). In the case of BIH, varying its concentration from the μM to mM range verified that both PF and TADF were efficiently quenched (Fig. S4† and 10) with large quenching constants, *i.e.*, $k_q = 2.7 \times 10^9$ M^{-1} s^{-1} and 1.5×10^8 M^{-1} s^{-1}, respectively.

On the other hand, 1.0 M of TEOA could not quench PF at all (Fig. S5†). Although TADF was quenched by TEOA, the rate constant ($k_q = 3.2 \times 10^4$ M^{-1} s^{-1}) is much smaller compared to that of BIH (Fig. S6†). These results are further supported by thermodynamic calculations. In fact, the reported E_{00} transition energies of the singlet and triplet excited states of **4DPAIPN** are 2.59 eV and 2.42 eV respectively,[37] the reduction potentials of the singlet and triplet excited states of **4DPAIPN** can be calculated as follows:

$$E(^1PS^*/PS^{\bullet-}) = E_{1/2}(PS/PS^{\bullet-}) + {}^1E_{00} = +0.51\ V\ vs.\ Fc^+/Fc \quad (1)$$

$$E(^3PS^*/PS^{\bullet-}) = E_{1/2}(PS/PS^{\bullet-}) + {}^3E_{00} = +0.34\ V\ vs.\ Fc^+/Fc \quad (2)$$

Since the oxidation potential of BIH is $E(BIH^{\bullet+}/BIH)$ = −0.09 V *vs.* Fc^+/Fc,[52] the electron transfer processes from BIH to the singlet and triplet excited states are highly exothermic and, given that $E(^1PS^*/PS^{\bullet-})$ is more positive than $E(^3PS^*/PS^{\bullet-})$, a higher quenching constant is expected for PF compared to TADF. In contrast, since $E(TEOA^{\bullet+}/TEOA)$ is ∼0.5 V *vs.* Fc^+/Fc (0.80 V *vs.* SCE),[53] reductive quenching of **4DPAIPN**'s T_1 and S_1 are both thermodynamically unfavorable or only slightly exergonic.

Furthermore, quenching fractions (η_q) can be calculated according to eqn (3):

$$\eta_q = k_q\tau^0[Q]/(1 + k_q\tau^0[Q]) \quad (3)$$

where k_q is the quenching constant, τ^0 is the emission lifetime in the absence of the quencher, and [Q] is the concentration of the quencher. Based on the quenching constant values obtained during Stern–Volmer experiments, when [BIH] = 0.1 M and in the absence of TEOA, the quenching efficiencies are $\eta_q^{PF} = 44\%$ and $\eta_q^{TADF} > 99\%$. That is, BIH almost quantitatively quenches the longer-lived triplet excited state of **4DPAIPN** (*i.e.*, TADF) and also about half of the singlet excited state that gives PF. In contrast, in the presence of only TEOA, no quenching of PF is possible even at [TEOA] = 1.5 M, whereas TADF is quenched with an efficiency of 80%. Nonetheless, under the reaction conditions employed in this work, TADF is quenched solely by BIH (>99%) because of the much faster quenching rate by BIH compared to that by TEOA (k_q[BIH] = 1.5×10^7 s^{-1} and k_q[TEOA] = 4.8×10^4 s^{-1}). The pathway involving oxidative quenching of the excited state of **4DPAIPN** by **Mn** can be ruled out on the basis of its low concentration ([**Mn**] = 50 μM). Moreover, the oxidation potential of the triplet excited state of **4DPAIPN** calculated using eqn (4) is almost equivalent to $E_p(\mathbf{Mn}/\mathbf{Mn}^{\bullet-})$ = −1.83 V, so oxidative quenching should be a slow process.

$$E(PS^{\bullet+}/{}^3PS^*) = E_{1/2}(PS^{\bullet+}/PS) - {}^3E_{00} = -1.87\ V\ vs.\ Fc^+/Fc \quad (4)$$

From these investigations, we can conclude that in the photocatalytic reaction using **4DPAIPN** the long-lived excited state of **4DPAIPN** is reductively quenched by BIH and the so-formed **4DPAIPN**$^{\bullet-}$ reduces **Mn**. It is noteworthy that the control experiment without BIH (entry 4 in Table 5) produced only trace amounts of CO and HCOOH, even though 80% of TADF is quenched by TEOA in the absence of BIH as described above. The possible reasons are the following: (1) the oxidized product of TEOA might react with **4DPAIPN** and/or **Mn** resulting in the loss of their function as a photosensitizer and/or catalyst;

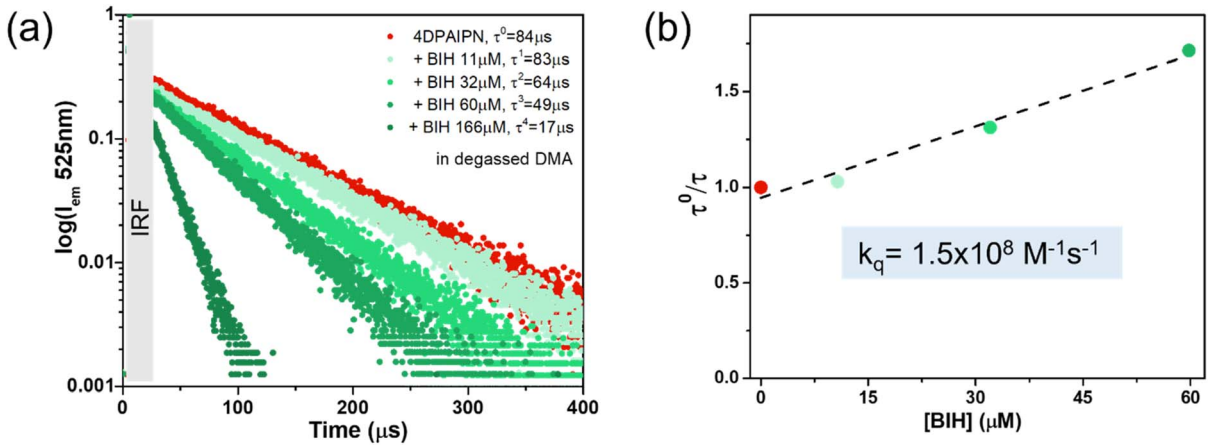

Fig. 10 (a) Emission intensity decays (λ_{ex}: 470 nm; λ_{em}: 525 nm) of **4DPAIPN** upon addition of increasing amounts of BIH (up to 166 μM) in degassed DMA. Instrument response function has been grayed-out. (b) Corresponding Stern–Volmer plot.

 This journal is © The Royal Society of Chemistry 2023

Open Access Article. Published on 27 June 2023. Downloaded on 2/10/2026 4:20:43 PM.
This article is licensed under a Creative Commons Attribution-NonCommercial 3.0 Unported Licence.

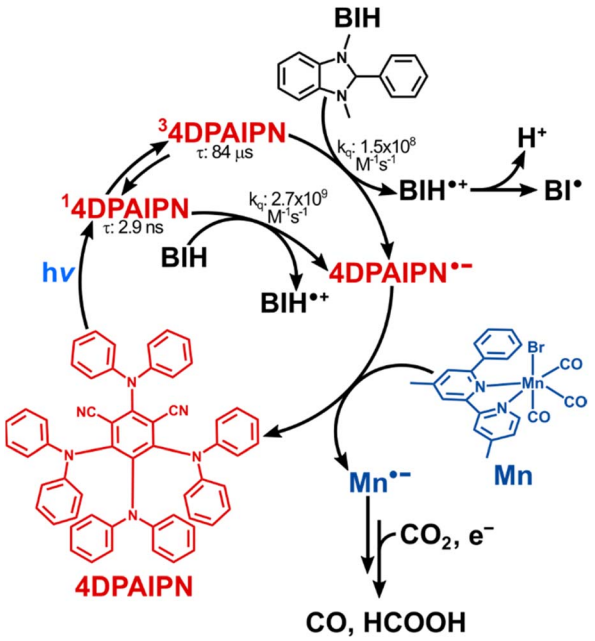

Fig. 11 Proposed mechanism for CO_2 reduction promoted by 4DPAIPN.

(2) as we previously reported, the slower quenching rate of the excited state might couple with more efficient back electron transfer in a solvated ion pair of [**4DPAIPN**$^{\bullet-}$···TEOA$^{\bullet+}$] resulting in a smaller quantum yield for the formation of **4DPAIPN**$^{\bullet-}$.[52]

On the basis of the experimental results described above, a hypothesis of the catalytic cycle that is active for the reduction of CO_2 promoted by **4DPAIPN** is reported in Fig. 11. The photocatalytic reduction is initiated by reductive quenching of both the singlet and triplet excited states of **4DPAIPN**, mainly by BIH. The so-obtained **4DPAIPN**$^{\bullet-}$ then efficiently donates one electron to **Mn**, thanks to its strong reduction power. The produced **Mn**$^{\bullet-}$ species might change its structure and react with CO_2, although the exact mechanisms of these processes have not been clarified yet. Interesting mechanistic points including the interaction between the Mn complex and TEOA[54,55] are currently under investigation in our laboratory. Finally, one more electron is supplied by BI$^\bullet$ (produced by deprotonation of BIH$^{\bullet+}$) and/or **4DPAIPN**$^{\bullet-}$ to the reaction intermediate made from **Mn**$^{\bullet-}$ to give CO and HCOOH.

Conclusions

A series of fully organic TADF molecules with diphenylamine (**4DPAIPN**, **3DPAFIPN**) or carbazole (**5CzBN**, **4CzIPN**, **3CzClIPN**) moieties as electron donating groups were systematically investigated as photoredox sensitizers for CO_2 reduction coupled to a new Mn(I) molecular catalyst (**Mn**). All of the investigated TADF molecules were reductively quenched by BIH in DMA–TEOA solutions. Since the one-electron reduced species of **4CzIPN** and **3CzClIPN** cannot supply an electron to **Mn** owing to their low reductive powers, they cannot work as photosensitizers in the studied photocatalytic system. Similarly, **5CzBN** cannot work as an efficient photosensitizer because of its low molar absorption coefficient in the visible region, even when using 440 nm light for irradiation. On the other hand, TADF molecules with diphenylamine groups are characterized by stronger absorption in the visible region and their one-electron reduced species have stronger reductive powers. In particular, **4DPAIPN** proved to be the most efficient and durable photosensitizer in the photocatalytic reactions consisting in a molar ratio of photosensitizer : catalyst = 1 : 1 ($TON_{CO+HCOOH}$ > 650). The quantum yield for CO_2 reduction was measured as 22.8 ± 1.5%, which, to the best of our knowledge, is the highest value among the reported photocatalytic systems for CO_2-reduction using organic TADF molecules as photosensitizers. This demonstrated that a high molar absorption coefficient and red-shifted absorption, in addition to negative reduction potentials, are all beneficial for the reaction. Moreover, mechanistic investigation proved that a long excited state lifetime is essential in order to favour the efficient bimolecular quenching processes of the photosensitizer, and that BIH is the species mainly responsible for its reductive quenching. One limit to the overall reaction's quantum yield is the photosensitizer's internal conversion ($S_1 \rightarrow S_0$) deactivation constant (in the order of 1×10^8 s^{-1}) and prompt fluorescence, which lead to fast deactivation of the photosensitizer before it has been able to interact with the other species present in the mixture. Development of TADF photosensitizers with lower non-radiative and radiative deactivation from the singlet excited state will therefore be beneficial for the improvement of the reaction's efficiency.

Conflicts of interest

The authors declare no conflict of interest.

Acknowledgements

The work was supported by JSPS KAKENHI Grant Number JP22K19081, JP20H00396, and JP17H06440 in Scientific Research on Innovative Areas "Innovations for Light-Energy Conversion (I4LEC)". Italian national projects (PRIN 2017 20174SYJAF, SURSUMCAT and PRIN2017 20172M3K5N, CHIRALAB) are acknowledged for financial support of this research. P. C., P. G. C., A. G., E. B., F. C., and S. P. also acknowledge the University of Bologna for financial support.

References

1 N. Armaroli and V. Balzani, *Angew. Chem., Int. Ed.*, 2007, **46**, 52–66.
2 G. Segev, J. Kibsgaard, C. Hahn, Z. J. Xu, W. S. Cheng, T. G. Deutsch, C. Xiang, J. Z. Zhang, L. Hammarström, D. G. Nocera, A. Z. Weber, P. Agbo, T. Hisatomi, F. E. Osterloh, K. Domen, F. F. Abdi, S. Haussener, D. J. Miller, S. Ardo, P. C. McIntyre, T. Hannappel, S. Hu, H. Atwater, J. M. Gregoire, M. Z. Ertem, I. D. Sharp, K.-S. Choi, J. S. Lee, O. Ishitani, J. W. Ager,

Open Access Article. Published on 27 June 2023. Downloaded on 2/10/2026 4:20:43 PM. This article is licensed under a Creative Commons Attribution-NonCommercial 3.0 Unported Licence.

R. R. Prabhakar, A. T. Bell, S. W. Boettcher, K. Vincent, K. Takanabe, V. Artero, R. Napier, B. R. Cuenya, M. T. M. Koper, R. Van De Krol and F. Houle, *J. Phys. D: Appl. Phys.*, 2022, **55**, 323003.

3 V. Balzani, G. Bergamini and P. Ceroni, *Angew. Chem., Int. Ed.*, 2015, **54**, 11320–11337.

4 Y. Yamazaki, H. Takeda and O. Ishitani, *J. Photochem. Photobiol., C*, 2015, **25**, 106–137.

5 Y. Tamaki, H. Takeda and O. Ishitani, *Molecular Technology*, Wiley, 2019, vol. 1, pp. 209–249.

6 A. M. Cancelliere, F. Puntoriero, S. Serroni, S. Campagna, Y. Tamaki, D. Saito and O. Ishitani, *Chem. Sci.*, 2020, **11**, 1556–1563.

7 R. Konduri, H. Ye, F. M. MacDonnell, S. Serroni, S. Campagna and K. Rajeshwar, *Angew. Chem., Int. Ed.*, 2002, **41**, 3185–3187.

8 C.-F. Leung and T.-C. Lau, *Energy Fuels*, 2021, **35**, 18888–18899.

9 K. E. Dalle, J. Warnan, J. J. Leung, B. Reuillard, I. S. Karmel and E. Reisner, *Chem. Rev.*, 2019, **119**, 2752–2875.

10 H. Takeda, C. Cometto, O. Ishitani and M. Robert, *ACS Catal.*, 2017, **7**, 70–88.

11 C. Steinlechner, A. F. Roesel, E. Oberem, A. Päpcke, N. Rockstroh, F. Gloaguen, S. Lochbrunner, R. Ludwig, A. Spannenberg, H. Junge, R. Francke and M. Beller, *ACS Catal.*, 2019, **9**, 2091–2100.

12 L. Rotundo, R. Gobetto and C. Nervi, *Curr. Opin. Green Sustainable Chem.*, 2021, **31**, 100509.

13 H. Yuan, B. Cheng, J. Lei, L. Jiang and Z. Han, *Nat. Commun.*, 2021, **12**, 1835.

14 A. Rosas-Hernández, C. Steinlechner, H. Junge and M. Beller, *Green Chem.*, 2017, **19**, 2356–2360.

15 L. Gracia, L. Luci, C. Bruschi, L. Sambri, P. Weis, O. Fuhr and C. Bizzarri, *Chem.–Eur. J.*, 2020, **26**, 9929–9937.

16 Y. Sakaguchi, A. Call, M. Cibian, K. Yamauchi and K. Sakai, *Chem. Commun.*, 2019, **55**, 8552–8555.

17 H. Takeda, K. Ohashi, A. Sekine and O. Ishitani, *J. Am. Chem. Soc.*, 2016, **138**, 4354–4357.

18 H. Takeda, Y. Monma, H. Sugiyama, H. Uekusa and O. Ishitani, *Front. Chem.*, 2019, **7**, 1–12.

19 X. Zhang, M. Cibian, A. Call, K. Yamauchi and K. Sakai, *ACS Catal.*, 2019, **9**, 11263–11273.

20 H. Takeda, H. Kamiyama, K. Okamoto, M. Irimajiri, T. Mizutani, K. Koike, A. Sekine and O. Ishitani, *J. Am. Chem. Soc.*, 2018, **140**, 17241–17254.

21 C. Bizzarri, *Eur. J. Org. Chem.*, 2022, e202200185.

22 J. Shipp, S. Parker, S. Spall, S. L. Peralta-Arriaga, C. C. Robertson, D. Chekulaev, P. Portius, S. Turega, A. Buckley, R. Rothman and J. A. Weinstein, *Inorg. Chem.*, 2022, **61**, 13281–13292.

23 J. Bonin, M. Robert and M. Routier, *J. Am. Chem. Soc.*, 2014, **136**, 16768–16771.

24 S. Matsuoka, K. Yamamoto, C. Pac and S. Yanagida, *Chem. Lett.*, 1991, **20**, 2099–2100.

25 S. Matsuoka, K. Yamamoto, T. Ogata, M. Kusaba, N. Nakashima, E. Fujita and S. Yanagida, *J. Am. Chem. Soc.*, 1993, **115**, 601–609.

26 T. Dhanasekaran, J. Grodkowski, P. Neta, P. Hambright and E. Fujita, *J. Phys. Chem. A*, 1999, **103**, 7742–7748.

27 L. Chen, Y. Qin, G. Chen, M. Li, L. Cai, Y. Qiu, H. Fan, M. Robert and T.-C. Lau, *Dalton Trans.*, 2019, **48**, 9596–9602.

28 H. Rao, J. Bonin and M. Robert, *ChemSusChem*, 2017, **10**, 4447–4450.

29 Z. Guo, S. Cheng, C. Cometto, E. Anxolabéhère-Mallart, S.-M. Ng, C.-C. Ko, G. Liu, L. Chen, M. Robert and T.-C. Lau, *J. Am. Chem. Soc.*, 2016, **138**, 9413–9416.

30 H. Rao, C.-H. Lim, J. Bonin, G. M. Miyake and M. Robert, *J. Am. Chem. Soc.*, 2018, **140**, 17830–17834.

31 T. Ogata, Y. Yamamoto, Y. Wada, K. Murakoshi, M. Kusaba, N. Nakashima, A. Ishida, S. Takamuku and S. Yanagida, *J. Phys. Chem.*, 1995, **99**, 11916–11922.

32 A. Juris, V. Balzani, F. Barigelletti, S. Campagna, P. Belser and A. von Zelewsky, *Coord. Chem. Rev.*, 1988, **84**, 85–277.

33 D. Sasikumar, A. T. John, J. Sunny and M. Hariharan, *Chem. Soc. Rev.*, 2020, **49**, 6122–6140.

34 J. Zhao, W. Wu, J. Sun and S. Guo, *Chem. Soc. Rev.*, 2013, **42**, 5323.

35 E. Bassan, A. Gualandi, P. G. Cozzi and P. Ceroni, *Chem. Sci.*, 2021, **12**, 6607–6628.

36 H. Uoyama, K. Goushi, K. Shizu, H. Nomura and C. Adachi, *Nature*, 2012, **492**, 234–238.

37 V. K. Singh, C. Yu, S. Badgujar, Y. Kim, Y. Kwon, D. Kim, J. Lee, T. Akhter, G. Thangavel, L. S. Park, J. Lee, P. C. Nandajan, R. Wannemacher, B. Milián-Medina, L. Lüer, K. S. Kim, J. Gierschner and M. S. Kwon, *Nat. Catal.*, 2018, **1**, 794–804.

38 E. Speckmeier, T. G. Fischer and K. Zeitler, *J. Am. Chem. Soc.*, 2018, **140**, 15353–15365.

39 M. A. Bryden and E. Zysman-Colman, *Chem. Soc. Rev.*, 2021, **50**, 7587–7680.

40 A. Gualandi, M. Anselmi, F. Calogero, S. Potenti, E. Bassan, P. Ceroni and P. G. Cozzi, *Org. Biomol. Chem.*, 2021, **19**, 3527–3550.

41 Y. Wang, X.-W. Gao, J. Li and D. Chao, *Chem. Commun.*, 2020, **56**, 12170–12173.

42 Y. Wang, T. Liu, L. Chen and D. Chao, *Inorg. Chem.*, 2021, **60**, 5590–5597.

43 Y. Wang, L. Chen, T. Liu and D. Chao, *Dalton Trans.*, 2021, **50**, 6273–6280.

44 T. Liu, Y. Li, Y. Fang, Y. Fu, Y. Chen and D. Chao, *Chem.–Asian J.*, 2022, **17**, e2022008, DOI: **10.1002/asia.202200846**.

45 Y. Fang, T. Liu, L. Chen and D. Chao, *Chem. Commun.*, 2022, **58**, 7972–7975.

46 Quantum yields were recalculated by using the following equations (see ref. 4) because reductants such as triethylamine used in ref. 39–43 are known to work as two-electron donor in one photosensitized cycle. Φ = (total number of products)/(number of photons).

47 M. Bourrez, F. Molton, S. Chardon-Noblat and A. Deronzier, *Angew. Chem., Int. Ed.*, 2011, **50**, 9903–9906.

48 M. D. Sampson, A. D. Nguyen, K. A. Grice, C. E. Moore, A. L. Rheingold and C. P. Kubiak, *J. Am. Chem. Soc.*, 2014, **136**, 5460–5471.

49 Y. Pellegrin and F. Odobel, *C. R. Chim.*, 2017, **20**, 283–295.

 This journal is © The Royal Society of Chemistry 2023

Open Access Article. Published on 27 June 2023. Downloaded on 2/10/2026 4:20:43 PM.
This article is licensed under a Creative Commons Attribution-NonCommercial 3.0 Unported Licence.

50 H. Koizumi, H. Chiba, A. Sugihara, M. Iwamura, K. Nozaki and O. Ishitani, *Chem. Sci.*, 2019, **10**, 3080–3088.
51 Y. Kuramochi, M. Kamiya and H. Ishida, *Inorg. Chem.*, 2014, **53**, 3326–3332.
52 K. Ozawa, Y. Tamaki, K. Kamogawa, K. Koike and O. Ishitani, *J. Chem. Phys.*, 2020, **153**, 154302.
53 K. Kalyanasundaram, *J. Chem. Soc., Faraday Trans. 2*, 1986, **82**, 2401.
54 T. Nakajima, Y. Tamaki, K. Ueno, E. Kato, T. Nishikawa, K. Ohkubo, Y. Yamazaki, T. Morimoto and O. Ishitani, *J. Am. Chem. Soc.*, 2016, **138**, 13818–13821.
55 T. Morimoto, T. Nakajima, S. Sawa, R. Nakanishi, D. Imori and O. Ishitani, *J. Am. Chem. Soc.*, 2013, **135**, 16825–16828.